

**Dynamics of Single-Molecule Dissociation by Selective Excitation of Molecular Phonons**Caiyun Chen,<sup>1,3,‡</sup> Longjuan Kong,<sup>1,3,‡</sup> Yu Wang,<sup>1,3</sup> Peng Cheng,<sup>1,3</sup> Baojie Feng,<sup>1</sup>  
Qijing Zheng,<sup>2</sup> Jin Zhao,<sup>2,5,\*</sup> Lan Chen<sup>①</sup>,<sup>1,3,4,†</sup> and Kehui Wu<sup>1,3,4</sup><sup>1</sup>*Institute of Physics, Chinese Academy of Sciences, Beijing 100190, China*<sup>2</sup>*ICQD/Hefei National Laboratory for Physical Sciences at Microscale,  
and CAS Key Laboratory of Strongly-Coupled Quantum Matter Physics,**and Department of Physics, University of Science and Technology of China, Hefei, Anhui 230026, China*<sup>3</sup>*School of Physics, University of Chinese Academy of Sciences, Beijing 100049, China*<sup>4</sup>*Songshan Lake Materials Laboratory, Dongguan, Guangdong 523808, China*<sup>5</sup>*Synergetic Innovation Center of Quantum Information and Quantum Physics,  
University of Science and Technology of China, Hefei, Anhui 230026, China*

(Received 2 January 2019; revised manuscript received 18 September 2019; published 13 December 2019)

Breaking bonds selectively in molecules is vital in many chemistry reactions and custom nanoscale device fabrications. The scanning tunneling microscope (STM) has proved to be an ideal tool to initiate and view bond-selective chemistry at the single-molecule level, offering opportunities for the further study of the dynamics in single molecules on metal surfaces. We demonstrate H—HS and H—S bond breaking on Au(111) induced by tunneling electrons using low-temperature STM. An experimental study combined with theoretical calculations shows that the dissociation pathway is facilitated by vibrational excitations. Furthermore, the dissociation probabilities of the two different dissociation processes are bias dependent due to different inelastic-tunneling probabilities, and they are also closely linked to the lifetime of inelastic-tunneling electrons. Combined with time-dependent *ab initio* nonadiabatic molecular dynamics simulations, the dynamics of the injected electron and the phonon-excitation-induced molecule dissociation can be understood at the atomic scale, demonstrating the potential application of STM for the investigation of excited-state dynamics of single molecules on surfaces.

DOI: 10.1103/PhysRevLett.123.246804

The excitation of molecular vibrations, e.g., phonons, plays an important role in various surface dynamic phenomena [1–9], for example, in molecular dissociation [9–11]. It can help the molecules overcome the activation barrier for chemical bond cleaving [12–15]. Scanning tunneling microscopy (STM) is a powerful technique for investigating chemical reactions on surfaces by initiating electronic and vibrational excitations in molecules by inelastic-tunneling (IET) electrons [9,10,16–22]. By controlling the energy and injection location of inelastic electrons, mode-selective chemical reactions on surfaces can be achieved by STM with high spatial and energy resolutions [21,23–25], which are perfect for studying single-molecule reactions on surfaces.

Most previous STM studies did not probe the dynamics of inelastic electron relaxations, phonon excitations, and surface chemical reactions because STM is generally used to measure the static atomic and electronic structures. Nevertheless, the outcome of the chemical reactions has strong correlation with the coherence dynamics of atoms and electrons. STM is able to estimate and regulate the femtosecond (fs) lifetime of excited electrons on single molecules [22,26], suggesting its capability of controlling single-molecule dynamics on surfaces. Yet, only a simple empirical model was previously used to estimate the

lifetime of excited states in the molecule. The comprehensive dynamics incorporating the chemical reaction with femtosecond time resolution is still challenging to model.

In this Letter, we study inelastic-electron-induced molecule dissociation of H<sub>2</sub>S on a Au(111) surface by combining the STM with time-resolved nonadiabatic molecular dynamics (NAMD) within the framework of the time-dependent Kohn-Sham equation [27]. The H<sub>2</sub>S molecule was chosen because H<sub>2</sub>S and its dissociation products have played an important role in electrochemistry, corrosion, environmental chemistry, and heterogeneous catalysis [43–45].

The H<sub>2</sub>S molecules physically adsorb on Au(111) [46–50], so we resolve only individual H<sub>2</sub>S molecules by STM at liquid helium temperature. Figure 1(a) is a large-area STM image of 0.01 monolayer H<sub>2</sub>S molecules adsorbed on Au(111) at 4.7 K. Individual H<sub>2</sub>S molecules on Au(111) appear as rounded protrusions in high-resolution images [Fig. 1(b)] and the apparent height is about 130 pm. The optimum configuration of an isolated H<sub>2</sub>S molecule on Au(111) from density functional theory (DFT) calculations [Fig. 1(d)] indicate that the H<sub>2</sub>S monomer adsorbs flat with the S atom located atop a Au atom. The distance between the S and Au atoms is 2.67 Å, corresponding to an adsorption energy of −0.5 eV, suggesting a relatively weak molecule-surface interaction.

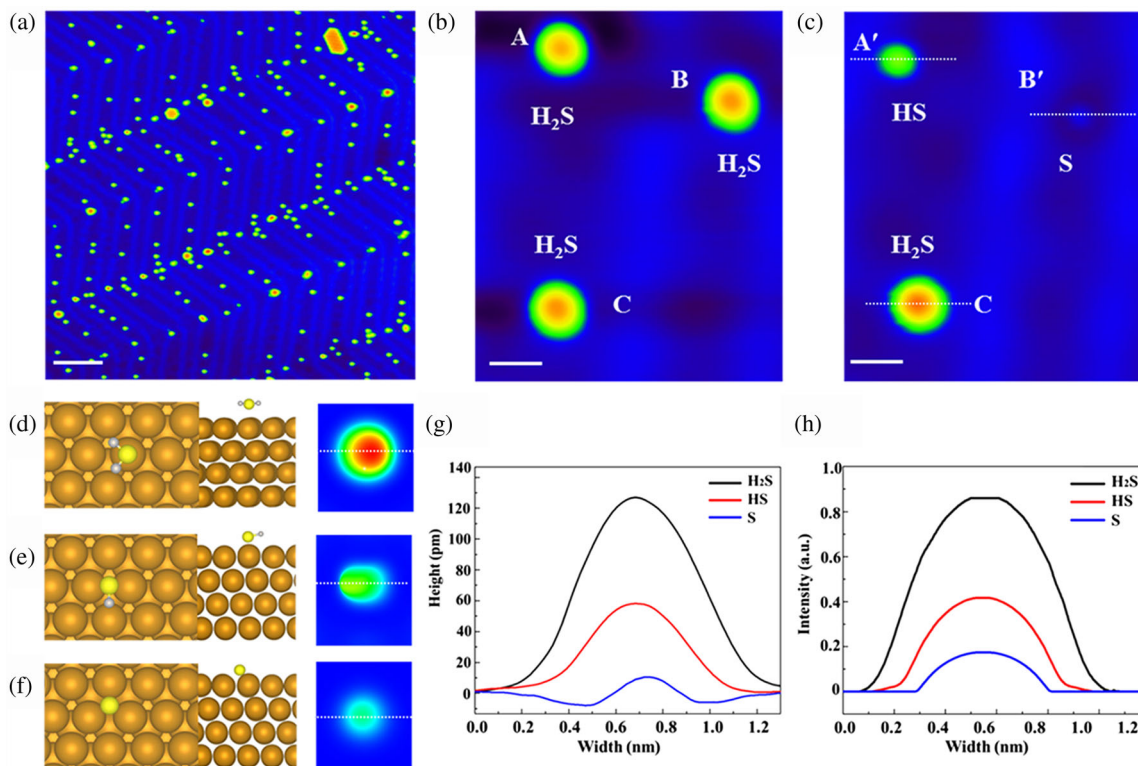


FIG. 1. (a) STM image of 0.01 monolayer  $\text{H}_2\text{S}$  molecules adsorbed on Au(111) surface. Scale bar, 10 nm. (b) STM image of isolated  $\text{H}_2\text{S}$  molecules marked by  $A$ ,  $B$ ,  $C$ . (c) STM image of the same area as (b) after applying pulses of  $-1.0$  V with tunneling currents of  $0.8$  nA on molecules  $A$  and  $B$ , which are dissociated to HS ( $A'$ ) and S ( $B'$ ), respectively. Scale bar, 1 nm. The scanning parameters of (a)–(c):  $V_{\text{tip}} = -100$  mV,  $I = 100$  pA. (d)–(f) The calculated results of single  $\text{H}_2\text{S}$ , HS, and S on Au(111), respectively. The left and middle panels are top and side views of relaxed structural models, in which the yellow, gray, and gold balls represent the S, H, and Au atoms, respectively. The right panels are simulated STM images. (g),(h) Line profiles along dotted lines in (c) and simulated  $\text{H}_2\text{S}$ , HS molecule, and S atom images at  $-100$  mV.

Applying a pulse ( $-1.0$  V,  $0.8$  nA,  $100$  ms) on the target  $\text{H}_2\text{S}$  molecule [labeled  $A$  in Fig. 1(b)] changes it to a ball-shaped and darker protrusion [ $A'$  in Fig. 1(c)] with a height of about  $65$  pm. By continuing to apply another pulse on the reacted molecule, a much darker dot with a height of  $7$  pm was obtained [ $B'$  in Fig. 1(c)]. Because of the simple stoichiometric ratio of the  $\text{H}_2\text{S}$  molecule, we postulate that the chemical reactions induced by STM pulses are the dissociation of  $\text{H}_2\text{S}$  and the dissociation of HS, respectively, and the reaction products are the HS molecule and the S atom, respectively.

The DFT calculation result of HS on Au(111) is shown in Fig. 1(e), indicating that the S atom in HS prefers to adsorb on the bridge site. The adsorption energy of HS is  $-2.16$  eV, which is much stronger than  $\text{H}_2\text{S}$  on Au(111). The optimized distance between the S atom and the Au atom is  $2.50$  Å. Moreover, the S atom is energetically favorable on the hollow-fcc adsorption site [Fig. 1(f)]. The corresponding simulated STM images of  $\text{H}_2\text{S}$ , HS, and S on Au(111) are shown in Figs. 1(d)–1(f) and Fig. S3 of the Supplemental Material (SM) [27], indicating the similar protrusions as experimental images. Furthermore, the line profiles along  $\text{H}_2\text{S}$ , the HS molecule and S atom shown in

Figs. 1(g) and 1(h) and Fig. S3 of the SM [27], reflect the height evolution from  $\text{H}_2\text{S}$  to S in both experimental measurements, and theoretical simulations can agree with each other qualitatively, suggesting that our proposed reacted products are reasonable. Similar DFT investigations for  $\text{H}_2\text{S}$ , HS, and S were previously reported [47–49].

To find out the dissociation reaction mechanism, we statistically analyzed the dissociation probability [in our experiments, the dissociation probability is defined as the ratio of the number of reaction events to the number of applied pulses ( $>100$  times) with the same energy, current, and duration time], as shown in Fig. 2. The energy onsets for the  $\text{H}_2\text{S} \rightarrow \text{HS}$  dissociation reactions on Au(111) are determined to be  $-0.33$  eV (electrons from tip to surface) and  $0.35$  eV (electrons from surface to tip), while the energy onsets for  $\text{HS} \rightarrow \text{S}$  dissociation are  $-0.38$  and  $1.25$  eV, respectively. The similar relative low energy onsets suggest the same mechanism for both dissociation reactions. However, the dissociation probability induced by positive pulses is clearly lower than for negative pulses, which might result from the different origins of tunneling electrons (i.e., electrons emitted from the tip or substrate). The screening effect of the substrate leads to a decreasing

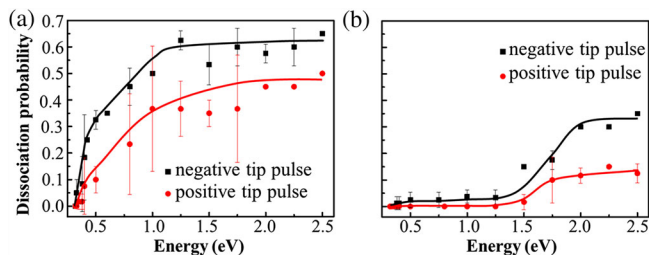


FIG. 2. (a),(b) The dissociation probability of isolated  $\text{H}_2\text{S}$  and HS on Au(111) surface induced by tip bias pulses, respectively. The black (red) lines indicate negative (positive) tip pulses applied on molecules. The probabilities are derived from the ratio of the number of dissociated molecules to the total number of trials ( $>100$  times) after pulsing with a certain bias, as well as the constant tunneling current of 0.8 nA and pulse duration of 100 ms.

IET probability, and consequently to a lower dissociation possibility [51,52]. The behaviors for these two dissociation reactions are different. For the  $\text{H}_2\text{S} \rightarrow \text{HS}$  dissociation, when the pulse energy is higher than the threshold, the dissociation probabilities increase quickly and are then saturated with energy higher than 1.25 eV [Fig. 2(a)]. For the  $\text{HS} \rightarrow \text{S}$  dissociation, the dissociation probabilities

remain low and increase only with an energy larger than 1.25 eV [Fig. 2(b)].

Our experimental results indicate that the chemical bond cleavage in adsorbates is attributed to the injection of tunneling electrons temporarily trapped by the molecular orbitals at the molecule-metal interface via an IET process, which can induce molecular dynamical processes such as lateral hopping [3,5], rotation [1,2], dissociation [9–11], desorption [23], and single-bond formation [53]. Thus, detailed knowledge of the electronic structures and molecular orbitals at the molecule-substrate interface is instructive for understanding the mechanism of chemical bond cleavage processes for  $\text{H}_2\text{S}$  (HS) on Au(111).

The total and projected density of states (PDOS), together with the spatial distribution of frontier molecular orbitals contributed by an isolated  $\text{H}_2\text{S}$  molecule both in the gas phase and on the Au (111) surface, are shown in Fig. 3(a). It is apparent that some small electronic states composed of  $3p_z$  orbitals of the S atom emerge near the Fermi level ( $E_F$ ) for a  $\text{H}_2\text{S}$  molecule on Au(111). For HS adsorbed on Au(111) [Fig. 3(b)], due to the stronger interactions between S and Au atoms, more pronounced hybridization of states occur near  $E_F$ . According to the PDOS shown in Fig. 3, the incident electrons with energies between 0.33 and 2.5 eV cannot transfer into the LUMO of

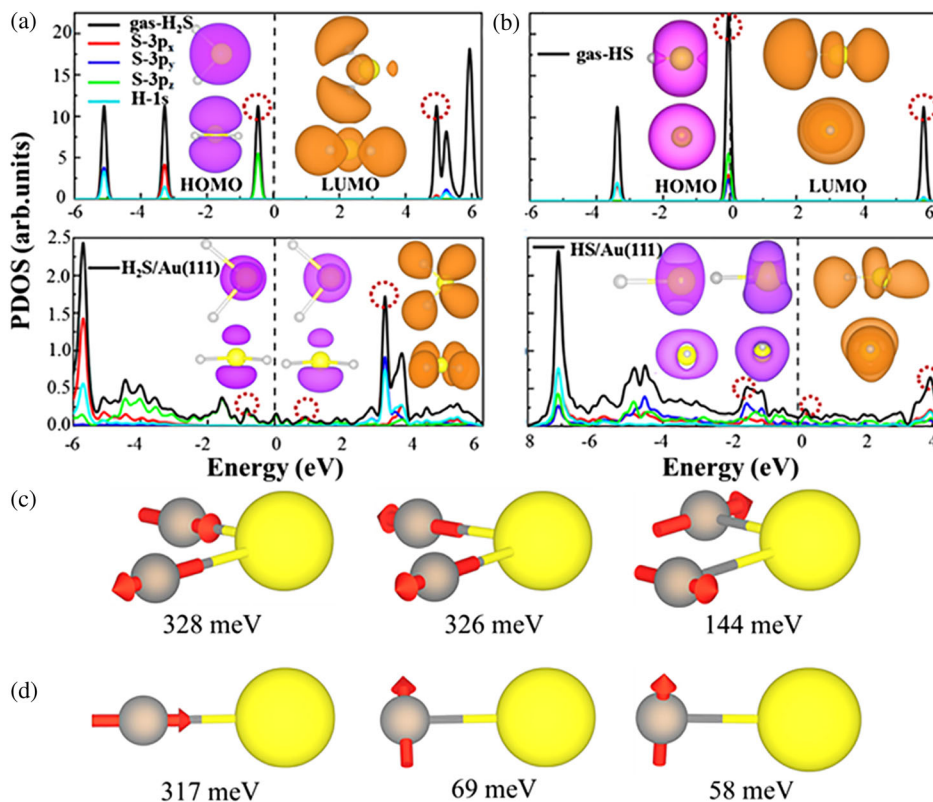


FIG. 3. (a) PDOS of  $\text{H}_2\text{S}$  (top panel) in gas phase and (bottom panel) on the Au surface. (b) PDOS of HS (top panel) in gas phase and (bottom panel) on the Au surface. The vertical black dashed lines denote the Fermi level. (Insets) Visualization of the spatial distribution of the main DOS peaks depicted by red dashed circles near Fermi level. (c),(d) Illustration of the vibrational modes of  $\text{H}_2\text{S}$  and the HS on Au surfaces, respectively. For a clear view, the Au(111) surface is hidden.

$\text{H}_2\text{S}$  ( $\sim 3.0$  eV) or HS ( $\sim 3.7$  eV) on the Au surface. This implies that the successive H–S bond cleavages are not ascribed to the weakened H–S bonds via electrons transferring to antibonding orbitals. Considering the low threshold bias for dissociation reactions (0.33 or 0.38 eV), we postulated that the H–S bond cleavages are associated with vibrational excitations.

To verify this hypothesis, we calculated the phonon modes of  $\text{H}_2\text{S}$  and HS molecules on Au(111), as shown in Figs. 3(c) and 3(d). The phonon energies of individual  $\text{H}_2\text{S}$  on Au (111) at 0.328, 0.326, and 0.14 eV correspond to the asymmetric stretch [ $\nu_a(\text{H}_2\text{S})$ ], symmetric stretch [ $\nu_s(\text{H}_2\text{S})$ ], and bending mode [ $\nu_b(\text{H}_2\text{S})$ ], respectively. Similarly, the stretching [ $\nu_s(\text{HS})$ ], perpendicular-to-surface rotation [ $\nu_r(\text{HS})$ ], and bending modes [ $\nu_b(\text{HS})$ ] of adsorbed HS are at 0.32, 0.069, and 0.058 eV, respectively. It is known that phonon modes of adsorbed molecules can be excited by the IET process [12–15]. The threshold bias 0.33 eV for  $\text{H}_2\text{S}$  dissociation matches the two stretching modes  $\nu_a(\text{H}_2\text{S})$  and  $\nu_s(\text{H}_2\text{S})$  well, while the threshold bias  $\sim 0.38$  eV for HS dissociation accords with the excitation energy of  $\nu_s(\text{HS})$  well. The perfect matches indicate that the  $\text{H}_2\text{S}$  and HS bond cleavages are induced by phonon excitation due to energy transfer from the IET electrons to the molecules.

The asymmetric and symmetric stretch modes for  $\text{H}_2\text{S}$  on Au(111) have nearly degenerate energies. It is intuitive that the asymmetric stretch mode should induce one H–S bond cleaving, while the symmetric stretch mode induces cleavage of two H–S bonds simultaneously. However, in experiments, two H–S bond cleaving reactions were not observed. To elucidate the origin of selectivity for the responsible vibration modes, we calculated the energy barriers for molecular dissociations by the climbing-image nudged elastic band (CI-NEB) method [34]. Two reaction pathways of H–S bond cleavage in the  $\text{H}_2\text{S}$  molecule are calculated. The barrier for the  $\text{H}_2\text{S} \rightarrow \text{H} + \text{HS}$  process on the Au(111) surface is  $\sim 0.83$  eV [Fig. 4(a)]. For  $\text{H}_2\text{S} \rightarrow \text{H} + \text{H} + \text{S}$ , the CI-NEB calculations are difficult to converge. This reaction tends to happen by breaking the two HS bonds one by one. To estimate the energy barrier, we simultaneously stretch the two HS bonds and allow the molecule to relax in the direction perpendicular to the surface (Fig. S11 in the SM) [27]. In this way, the energy barrier for the simultaneous dissociation is estimated at 2.31 eV. The much higher energy barrier for two H–S bonds cleaving simultaneously explains why that reaction is not observed in experiments. In addition, as shown in Figs. 4(c) and 4(d), the calculated energy barrier for the  $\text{HS} \rightarrow \text{H} + \text{S}$  process is  $\sim 0.89$  eV.

Comparing the dissociation barrier (0.83 or 0.89 eV) with the threshold bias 0.33 or 0.38 eV, multiple phonons should be excited to overcome the dissociation barrier. The proposed microscopic picture can be verified by tracing the trajectory of the variation of H–S bond lengths in a

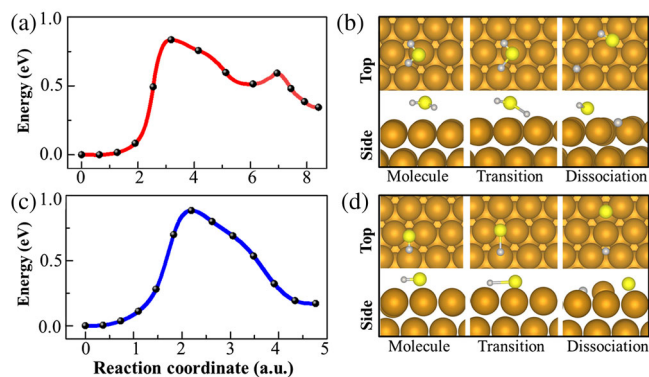


FIG. 4. Reaction energy profile and atomic structure models along the reaction path of (a),(b) an  $\text{H}_2\text{S}$  on Au(111) dissociating into  $\text{HS} + \text{H}$ , and (c),(d) a HS monomer on Au(111) with  $\text{H} + \text{S}$  dissociated products.

molecular dynamics (MD) simulation. Our simulations reveal that when four phonons are excited, the lengths of two H–S bonds oscillate for three periods, and then one of them elongates gradually, leading to single-bond breaking at  $\sim 70$  fs [Fig. 5(a)]. Figures 5(b)–5(e) give the time evolution geometries for  $\text{H}_2\text{S}$  on Au(111) at 35 fs intervals. After 35 fs [Fig. 5(c)], one H atom tilts toward the Au surface, and its distance from S is elongated until it breaks away from the HS fragment at 70 fs [Fig. 5(d)]. The case for the dissociation of HS on Au(111) is similar, as shown in Figs. 5(f)–5(j) and Figs. S5(a)–S5(c) in the SM [27]. The excitation of four phonons is also required for the HS dissociation reaction. The frequencies of different phonon modes can also be obtained from the Fourier transform spectra from the NAMD simulation, agreeing with static DFT calculations [27]. Based on the potential barrier values estimated by the CI-NEB method, three phonons with energy of 0.33 eV (0.32 eV) for  $\text{H}_2\text{S}$  (HS) are, in principle, sufficient to overcome the reaction barriers for dissociation in a vibrational ladder climbing manner [54]. However, the direction of the S-H stretching mode excited by IET

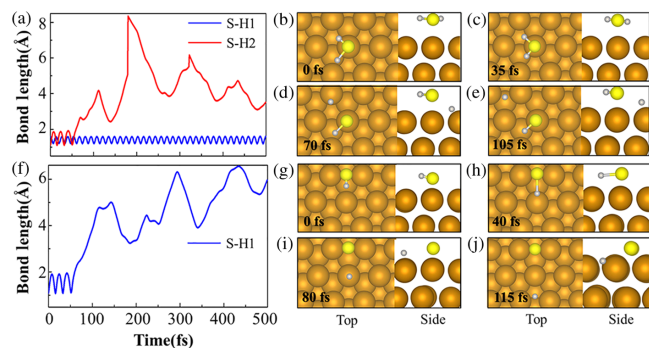


FIG. 5. The time-dependent HS bond length evolutions in a 500 fs *ab initio* molecular dynamics simulation for (a) a  $\text{H}_2\text{S}$  molecule on a Au surface and (f) HS on Au. The computed trajectories of H–S bond breaking in (b)–(e) an isolated  $\text{H}_2\text{S}$  molecule and (g)–(j) isolated HS adsorbed on Au(111).

electrons is different from the reaction coordinate of the CI-NEB, and the dynamic behavior of dissociation by vibrational excitation is not completely along the CI-NEB path with the lowest energy barrier (Fig. S7 in the SM [27]). The dissociated process should involve a higher effective barrier height for four phonons to climb up.

Therefore, we deduce that the dissociation pathway of  $\text{H}_2\text{S}$  on Au(111) comprises four phonons with asymmetric stretching modes excited by inelastic electrons. Below a bias of 1.25 eV, more than one electron is needed for the four phonons' excitation. The energy of a single inelastic electron above 1.25 eV is sufficient to excite four phonons to overcome a dissociation barrier, which explains why the dissociation probability is saturated when the pulse bias is larger than  $\sim 1.25$  eV. The case of HS is similar to  $\text{H}_2\text{S}$ . The variation of probability with bias also indicates that energy transfers from more than one tunneling electron are required to break the H—S bond at low bias. Using equilibrium molecular dynamics simulations and normal mode decomposition [39], the lifetime of the asymmetric stretching mode of  $\text{H}_2\text{S}$  due to the anharmonic phonon-phonon interaction is estimated to be 704 fs [27], which is much longer than the timescale of  $\text{H}_2\text{S}$  dissociation, supporting the phonon-induced molecular dissociation postulate. During the dissociation processes of  $\text{H}_2\text{S}$  and HS, due to the anharmonic coupling between different phonon modes, the energy transfers to other modes like the Au-S and Au-Au stretching modes. All of these modes play a role in the dissociation. However, since the dissociation timescale is much shorter than the phonon lifetime, we think that the anharmonic effects within such a short timescale are not significant.

The molecular phonons are excited by IET electrons trapped in hybridized states of a molecule near  $E_F$ . Therefore, the lifetime of injected electrons in hybridized states will influence the dissociation probability. We employed time-dependent *ab initio* NAMD to elucidate the dynamics of injected electrons in  $\text{H}_2\text{S}$  and HS molecules on Au(111). First, we plotted the time-dependent energy evolution of selected states in 2 ps MD at 100 K (Figs. S8 and S9 in the SM [27]). For both  $\text{H}_2\text{S}$  and HS on Au(111), the adiabatic electron-phonon coupling induces the fluctuation of these Kohn-Sham eigenenergies. The lifetime is determined to be the time interval of the electron relaxation from hybridized states to  $E_F$ . Figure 6 shows the variation of the lifetime with the initial energy of injected electrons on the  $\text{H}_2\text{S}$  and HS molecules, respectively. The lifetime of the electron on HS is always shorter than  $\text{H}_2\text{S}$  by 0.3–1.2 eV, and the largest difference occurs at 0.6–0.7 eV. The lifetimes of both  $\text{H}_2\text{S}$  and HS are similar at 0.33 or 1.25 eV, which are close to the threshold and saturation energies for the  $\text{H}_2\text{S}$  dissociation. The stronger hybridization between HS and the Au(111) surface generates a higher density of states in the relevant energy region [Fig. 3(b) and Fig. S9 in the SM [27]]. It contributes more

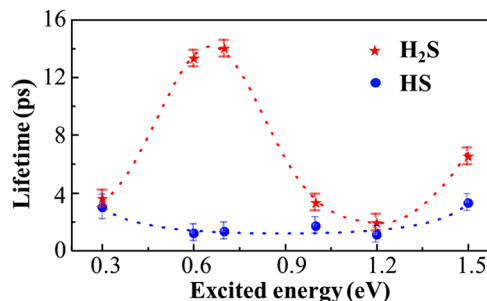


FIG. 6. The lifetime of an excited-state electron initially generated via an IET process of  $\text{H}_2\text{S}$  and a HS molecule on Au(111) with different initial energies at 100 K. The red and blue dotted lines are fits to the calculated data points.

efficient cooling channels for excited electron relaxing, and it reduces the lifetime of the HS molecule progressing on the excited-state potential energy surface from 0.38 to 1.25 eV. The short-lived travel of HS in the excited state cannot provide enough time to accumulate four vibrational modes of  $\nu_s(\text{HS})$  to overcome the dissociation barrier, explaining the low-value plateaus of dissociation probability for HS [Fig. 2(b)]. In addition, the higher probability for  $\text{H}_2\text{S}$  dissociation saturates at  $\sim 1.25$  eV, corresponding to the short lifetime of tunneling electron. By this token, the excited-state lifetime of the injected electron and the adsorbed molecular dissociation probability have positive correlations in the low bias range.

The reaction probability in molecule-surface systems is closely associated with the excited-state lifetimes [22,26,55,56], which were generally measured by time-resolved photoemission or optical techniques [57–60]. Although the time resolution can be achieved in those measurements, spatial resolution at atomic level is difficult to achieve. A recent study showed that the proximity of the STM tip suppresses the reaction probability by reducing the excited-state lifetime [22], suggesting the potential of STM to measure and control the coherent dynamics of excited carriers at the molecule-solid interface. Nevertheless, the excited-carrier lifetime was estimated only qualitatively. Here we quantitatively correlate the lower reaction probability of HS on Au(111) to the reduction of excited-state lifetimes. The lifetimes of injected electrons and the time-scale of chemical reactions induced by inelastic electrons can therefore be measured. Hence, the STM technique and time-dependent *ab initio* NAMD simulations may be widely extended to understand the coherent dynamics of injected-electron-induced chemical reactions on surfaces.

We thank Professor Sheng Meng from IOP for the useful discussion about the DFT calculations, and Professor Andrew Wee from NUS for his help with analysis of the experimental data. This work was supported by the MOST of China (Grants No. 2016YFA0202301, No. 2017YFA0204904, No. 2018YFE0202700, No. 2016YFA0200604, and No. 2016YFA0300904), the

NSF of China (Grants No. 11761141013, No. 11674366, No. 11674368, No. 11620101003, No. 11704363), the Beijing Natural Science Foundation (Grant No. Z180007), and the Strategic Priority Research Program of the Chinese Academy of Sciences (Grants No. XDB07010200 and No. XDB30000000).

\*zhaojin@ustc.edu.cn

†lchen@iphy.ac.cn

‡These authors contributed equally to this work.

- [1] B. C. Stipe, M. A. Rezaei, and W. Ho, *Phys. Rev. Lett.* **81**, 1263 (1998).
- [2] B. C. Stipe, M. A. Rezaei, and W. Ho, *Science* **279**, 1907 (1998).
- [3] T. Komeda, Y. Kim, M. Kawai, B. N. J. Persson, and H. Ueba, *Science* **295**, 2055 (2002).
- [4] Y. Sainoo, Y. Kim, T. Okawa, T. Komeda, H. Shigekawa, and M. Kawai, *Phys. Rev. Lett.* **95**, 246102 (2005).
- [5] J. Oh, H. Lim, R. Arafune, J. Jung, M. Kawai, and Y. Kim, *Phys. Rev. Lett.* **116**, 056101 (2016).
- [6] J. Mielke, J. Martínez-Blanco, M. V. Peters, S. Hecht, and L. Grill, *Phys. Rev. B* **94**, 035416 (2016).
- [7] A. Shiotari, T. Odani, and Y. Sugimoto, *Phys. Rev. Lett.* **121**, 116101 (2018).
- [8] Y. Kim, T. Komeda, and M. Kawai, *Phys. Rev. Lett.* **89**, 126104 (2002).
- [9] M. Ohara, Y. Kim, S. Yanagisawa, Y. Morikawa, and M. Kawai, *Phys. Rev. Lett.* **100**, 136104 (2008).
- [10] H. J. Shin, J. Jung, K. Motobayashi, S. Yanagisawa, Y. Morikawa, Y. Kim, and M. Kawai, *Nat. Mater.* **9**, 442 (2010).
- [11] B. C. Stipe, M. A. Rezaei, W. Ho, S. Gao, M. Persson, and B. I. Lundqvist, *Phys. Rev. Lett.* **78**, 4410 (1997).
- [12] S. Gao, M. Persson, and B. I. Lundqvist, *Phys. Rev. B* **55**, 4825 (1997).
- [13] S. G. Tikhodeev and H. Ueba, *Surf. Sci.* **587**, 25 (2005).
- [14] S. G. Tikhodeev and H. Ueba, *Phys. Rev. Lett.* **102**, 246101 (2009).
- [15] T. Frederiksen, M. Paulsson, and H. Ueba, *Phys. Rev. B* **89**, 035427 (2014).
- [16] H. Gawronski, K. Morgenstern, and K. H. Rieder, *Eur. Phys. J. D* **35**, 349 (2005).
- [17] J. Lee, D. C. Sorescu, and X. Deng, *J. Am. Chem. Soc.* **133**, 10066 (2011).
- [18] S. Tan, Y. Zhao, J. Zhao, Z. Wang, C. Ma, A. Zhao, B. Wang, Y. Luo, J. Yang, and J. Hou, *Phys. Rev. B* **84**, 155418 (2011).
- [19] T. Kudernac, N. Ruangsupapichat, M. Parschau, B. Maciá, N. Katsonis, S. R. Harutyunyan, K. H. Ernst, and B. L. Feringa, *Nature (London)* **479**, 208 (2011).
- [20] L. Lauhon and W. Ho, *Surf. Sci.* **451**, 219 (2000).
- [21] B. Jiang, D. Xie, and H. Guo, *Chem. Sci.* **4**, 503 (2013).
- [22] K. R. Rusimova, R. M. Purkiss, R. Howes, F. Lee, S. Crampin, and P. A. Sloan, *Science* **361**, 1012 (2018).
- [23] J. I. Pascual, N. Lorente, Z. Song, H. Conrad, and H. P. Rust, *Nature (London)* **423**, 525 (2003).
- [24] K. Motobayashi, Y. Kim, H. Ueba, and M. Kawai, *Phys. Rev. Lett.* **105**, 076101 (2010).
- [25] K. Motobayashi, Y. Kim, R. Arafune, M. Ohara, H. Ueba, and M. Kawai, *J. Chem. Phys.* **140**, 194705 (2014).
- [26] W. Paul, K. Yang, S. Baumann, N. Romming, T. Choi, C. P. Lutz, and A. J. Heinrich, *Nat. Phys.* **13**, 403 (2017).
- [27] See Supplemental Material at <http://link.aps.org/supplemental/10.1103/PhysRevLett.123.246804>, which includes Refs. [28–42], for details of experimental and calculational methods, as well as detailed calculated data.
- [28] G. Kresse and J. Hafner, *Phys. Rev. B* **47**, 558 (1993).
- [29] G. Kresse and J. Furthmüller, *Phys. Rev. B* **54**, 11169 (1996).
- [30] S. Grimme, J. Antony, S. Ehrlich, and H. Krieg, *J. Chem. Phys.* **132**, 154104 (2010).
- [31] S. Grimme, S. Ehrlich, and L. Goerigk, *J. Comput. Chem.* **32**, 1456 (2011).
- [32] J. P. Perdew, K. Burke, and M. Ernzerhof, *Phys. Rev. Lett.* **77**, 3865 (1996).
- [33] G. Kresse and D. Joubert, *Phys. Rev. B* **59**, 1758 (1999).
- [34] G. Henkelman, B. P. J. Uberuaga, and H. Jónsson, *J. Chem. Phys.* **113**, 9901 (2000).
- [35] L. Qi, X. Qian, and J. Li, *Phys. Rev. Lett.* **101**, 146101 (2008).
- [36] J. Behler, B. Delley, S. Lorenz, K. Reuter, and M. Scheffler, *Phys. Rev. Lett.* **94**, 036104 (2005).
- [37] Q. Z. Zheng and J. Zhao, <http://staff.ustc.edu.cn/~zhaojin/code.html>.
- [38] X. Meng, J. Guo, J. Peng, J. Chen, Z. Wang, J. Shen, X. Li, E. Wang, and Y. Jiang, *Nat. Phys.* **11**, 235 (2015).
- [39] A. J. H. McGaughey and J. M. Larkin, *Annual review of heat transfer* **17**, 49 (2014).
- [40] S. P. Rittmeyer, J. Meyer, J. I. Juaristi, and K. Reuter, *Phys. Rev. Lett.* **115**, 046102 (2015).
- [41] D. Novko, M. Blanco-Rey, J. I. Juaristi, and M. Alducin, *Phys. Rev. B* **92**, 201411(R) (2015).
- [42] I. Lončarić, M. Alducin, J. I. Juaristi, and D. Novko, *J. Phys. Chem. Lett.* **10**, 1043 (2019).
- [43] H. F. Prest, W. B. Tzeng, J. M. Brom, Jr., and C. Y. Ng, *J. Am. Chem. Soc.* **105**, 7531 (1983).
- [44] J. H. Chang, A. Huzayyin, K. Lian, and F. Dawson, *Phys. Chem. Chem. Phys.* **17**, 588 (2015).
- [45] X. Zhang, Y. Tang, S. Qu, J. Da, and Z. Hao, *ACS Catal.* **5**, 1053 (2015).
- [46] A. J. Leavitt and T. P. Beebe, Jr., *Surf. Sci.* **314**, 23 (1994).
- [47] P. N. Abufager, P. G. Lustemberg, C. Crespos, and H. F. Busnengo, *Langmuir* **24**, 14022 (2008).
- [48] N. Liu, X. Y. Wang, and Y. L. Wan, *J. Theor. Comput. Chem.* **13**, 1450065 (2014).
- [49] D. R. Alfonso, *Surf. Sci.* **602**, 2758 (2008).
- [50] H. Sellers, *Surf. Sci.* **294**, 99 (1993).
- [51] D. Šestović and M. Šunjić, *Solid State Commun.* **98**, 375 (1996).
- [52] D. Šestović, L. Marušić, and M. Šunjić, *Phys. Rev. B* **55**, 1741 (1997).
- [53] H. J. Lee and W. Ho, *Science* **286**, 1719 (1999).
- [54] Y. Kim, K. Motobayashi, T. Frederiksen, H. Ueba, and M. Kawai, *Prog. Surf. Sci.* **90**, 85 (2015).
- [55] P. Saalfrank, G. Boendgen, C. Corriol, and T. Nakajima, *Faraday Discuss.* **117**, 65 (2000).

- [56] J. Repp, G. Meyer, F. E. Olsson, and M. Persson, *Science* **305**, 493 (2004).
- [57] K. Onda, B. Li, J. Zhao, K. D. Jordan, J. Yang, and H. Petek, *Science* **308**, 1154 (2005).
- [58] B. Li, J. Zhao, K. Onda, K. D. Jordan, J. Yang, and H. Petek, *Science* **311**, 1436 (2006).
- [59] J. T. Yates and H. Petek, *Chem. Rev.* **106**, 4113 (2006).
- [60] H. Petek and J. Zhao, *Chem. Rev.* **110**, 7082 (2010).